

รายงานวิจัยฉบับสมบูรณ์

การใช้ทฤษฎีความคล้ายในการทำนายพฤติกรรมการโก่งงอของโครงสร้างแผ่นบางจาก

ผลการทดลองบนแบบจำลอง

Using the similitude theory to predict buckling behaviors of thin prototype plates from experiments of model plates

ไพโรจน์ สิงหถนัดกิจ และคณะ

รายงานวิจัยฉบับสมบูรณ์

การใช้ทฤษฎีความคล้ายในการทำนายพฤติกรรมการโก่งงอของโครงสร้างแผ่นบางจาก ผลการทดลองบนแบบจำลอง

Using the similitude theory to predict buckling behaviors of thin prototype plates from experiments of model plates

ไพโรจน์ สิงหถนัดกิจ จุฬาลงกรณ์มหาวิทยาลัย (หัวหน้าโครงการ)
วริทธิ์ อึ๊งภากรณ์ จุฬาลงกรณ์มหาวิทยาลัย (นักวิจัยที่ปรึกษา)

สนับสนุนโดยทบวงมหาวิทยาลัย และ สำนักงานกองทุนสนับสนุนการวิจัย
(ความเห็นในรายงานนี้เป็นของผู้วิจัย ทบวงฯ และ สกว. ไม่จำเป็นต้องเห็นด้วยเสมอไป)

บทคัดย่อ

ทฤษฎีความคล้ายถกนำมาใช้กับปัณหาการ โก่งงอของแผ่นคอม โพสิตบาง โดยทำการเปลี่ยน รูปด้านความคล้ายของสมการครอบคลุมเชิงอนุพันธ์โดยตรง การศึกษานี้ศึกษาแผ่นลามิเนตคอม โพสิตรูปสี่เหลี่ยมผืนผ้าและแผ่นรูปวงแหวนออโธโทรปิคแบบขั้ว โดยจะได้กฎสัดส่วนสำหรับแต่ ละปัญหาพร้อมทั้งข้อกำหนดความคล้ายระหว่างแบบจำลองและต้นแบบ กฎสัดส่วนที่ได้มาถูก ตรวจสอบความถูกต้องกับคำตอบที่มีอยู่ โดยการแทนค่าภาระการโก่งงอของแบบจำลองลงในกฎ สัคส่วนเพื่อหาภาระการ โก่งงอสัคส่วนของต้นแบบซึ่งจะนำ ไปเปรียบเทียบกับคำตอบทางทฤษฎี เพื่อหาความแม่นยำของกฎสัดส่วนในที่สด การทำนายโดยใช้กฎสัดส่วนให้ผลตรงกับค่าภาระการ โก่งงอทางทฤษฎีสำหรับกรณีคล้ายสมบรณ์ พบความคลาดเคลื่อนเล็กน้อยสำหรับกรณีของคล้าย บางส่วนที่แนะนำให้ใช้ได้ มีการตรวจสอบโดยการทดลองบนชุดทดลองการกดที่สร้างขึ้นเอง ชิ้นงานที่ใช้ในการศึกษาเป็นแผ่นคอมโพสิตรูปสี่เหลี่ยมผืนผ้าที่มีเงื่อนไขขอบเขตรวมกันของแบบ ธรรมดาหรือแบบอิสระ และมีการวางเรียงแบบ $[0/90]_{2s}$ $[0_{2}/90_{2}]_{2s}$ และ $[0/90]_{4s}$ การกระจายของ เปอร์เซ็นต์ความแตกต่างของภาระการโก่งงอจากกฎสัดส่วนและจากการทดลองสำหรับกรณีคล้าย สมบูรณ์และคล้ายบางส่วนพิจารณาได้ว่ามีการกระจายแบบปรกติ เปอร์เซ็นต์ความแตกต่างเฉลี่ย สำหรับกรณีคล้ายสมบูรณ์และคล้ายบางส่วนมีค่าเป็น -4.75 และ 10.7% ตามลำคับ พบว่ามีค่า ความเบี่ยงเบนของเปอร์เซ็นต์ความแตกต่างอยู่ในระดับปานกลาง จากการศึกษากรณีคล้ายสมบูรณ์ 30 คู่พบว่า 23 คู่ของชิ้นงานแบบจำลองและต้นแบบมีเปอร์เซ็นต์ความแตกต่างอยู่ในช่วง $\pm 10\%$ สำหรับกรณีของคล้ายบางส่วนชิ้นงานแบบจำลองและต้นแบบ 30 จาก 40 คู่มีเปอร์เซ็นต์ความแตก ต่างอยู่ในช่วง 0 ถึง +30% คังนั้นกฎสัคส่วนที่พิสูจน์มาได้รับการยืนยันด้วยทฤษฎีและการทคลอง กฎสัคส่วนนี้มีประโยชน์สำหรับการประเมินภาระการโก่งงอของแผ่นชิ้นงานที่มีเงื่อนไขขอบเขต ซับซ้อนและไม่ต้องการทดสอบบนชิ้นงานขนาดจริง

Abstract

The similitude theory is employed to buckling of composite plate problems by applying a similitude transformation directly to the differential governing equations. Rectangular laminated composite plates and polar orthotropic annular plates are investigated in this study. The scaling laws for each problem along with similarity requirements between model and prototype specimens are obtained. The derived scaling laws are theoretical verified with available solutions. The theoretical buckling load of a model is substituted into the scaling law to determine the scaling buckling load of a prototype, which is then compared to the theoretical solutions to determine the accuracy of the scaling law. In case of complete similitude, predictions from the derived scaling laws are identical to the theoretical buckling load. Small percent of discrepancy is observed for cases of recommended partial similitude. Experimental verification was also performed on a custom-made compression test frame. Specimens used in the study are rectangular composite plates with a combination of simple and free boundary conditions and stacking sequences of $[0/90]_{2s}$, $[0_2/90_2]_{2s}$, and $[0/90]_{4s}$. The distribution of percent discrepancy between scaling and experimental buckling loads for both complete and partial similitude cases is considered as a normal distribution. The average percent discrepancy of complete similitude and partial similitude are -4.75 and 10.7%, respectively. A moderate deviation of the percent discrepancy is observed from the study. Out of thirty pairs, twenty-three pairs of model-prototype specimens have percent discrepancy within $\pm 10\%$ for complete similitude case. In case of partial similitude, 30 out of 40 model-prototype pairs have percent discrepancy in the range of 0 to +30%. Therefore, the derived scaling laws are confirmed theoretically and experimentally. They are useful to estimate buckling of plates with complicate boundary conditions which full-scaled test is not preferred.

Keywords: buckling, composite material, similitude, scaling law, experiment

Executive Summary

Several studies devoted to buckling of composite plate are available in the literatures. Some experimental studies found a moderately high degree of discrepancy of experimental buckling loads compared with theoretical solutions. Imperfection of plate and boundary condition of the specimens are frequently mentioned as sources of the inconsistency. So there is a need for a better approach to predict the buckling load of plates with imperfections or plates with complicated configurations. This research project studies similitude theory as applied to buckling of composite plate problems. The project classifies into three sections; deriving the scaling law, verifying the scaling law with the experiment.

In the first part, the similitude theory is employed to buckling of composite plate problems. It is different from the previous studied by other researchers for the reason that, in this study, a similitude transformation was applied directly to the differential governing equations, not to the solutions of the equations as before. In the present study, rectangular laminated composite plates and polar orthotropic annular plates were investigated. The scaling laws for each problem along with similarity requirements between model and prototype specimens are obtained. The complete similitude requirements include geometric similarity, identical load ratio, and identical stiffness scaling factor. The scaling laws are independent of boundary conditions, i.e. they are applicable providing that boundary conditions of both systems are identical.

The second part of the project is to verify the derived scaling laws with available theoretical solutions. For rectangular plates, the available theoretical

solutions are analytical solutions in form of closed-form solutions and the semianalytical-numerical Ritz solutions. Only the Ritz method is applicable for annular
plate problem. The theoretical buckling load of a model is substituted into the scaling
law to determine the scaling buckling load of the prototype. Then, the scaling buckling
load is compared to the theoretical solution to determine the accuracy of the scaling
law. For complete similitude case, predictions from the derived scaling laws are
identical to the theoretical buckling load. In practice, it might be difficult or costly to
set up a model experiment which is completely satisfied the similarity requirements
for a particular prototype. Some similarity requirements could be dropped to avoid
expensive experiment. Applying the scaling law in this fashion is called partial
similitude. From the numerical calculation, a small percent of discrepancy is observed
for cases of recommended partial similitude.

In the final part of the project, experimental verification was performed on a custom-made compression test frame. The test setup is capable of applying a uniform compression on a rectangular specimen, and supporting the specimen with simply supported boundary conditions. Specimens used in the study are rectangular composite plates with a combination of simple and free boundary conditions and stacking sequences of $[0/90]_{2s}$, $[0_2/90_2]_{2s}$, and $[0/90]_{4s}$. The distribution of percent discrepancy between scaling and experimental buckling loads for both complete and partial similitude cases is considered as a normal distribution. The average percent discrepancy of complete similitude and partial similitude are -4.75 and 10.7%, respectively. A moderate deviation of the percent discrepancy is observed from the study. Out of thirty pairs, twenty-three pairs of model-prototype specimens have percent discrepancy within $\pm 10\%$ for complete similitude case. In case of partial similitude, 30 out of 40 model-prototype pairs have percent discrepancy in the range

of 0 to +30%. Therefore, the derived scaling laws are confirmed theoretically and experimentally. They are useful to estimate buckling of plates with complicate boundary conditions where full-scaled test is not desirable.

The outputs of this research project up to now are:

- Singhatahadgid, P. and, Ungbhakorn, V. "Scaling laws for buckling of polar orthotropic annular plates subjected to compressive and torsional loading," Accepted for publication in Thin-Walled Structures.
- Arunpitak, S., Singhatanadgid, P. and Ungbhakorn, V. "An experiment verification of the scaling law for buckling of cross-ply composite plates," Proceedings of the 18th Conference of the Mechanical Engineering Network of Thailand (ME-NETT 18). Sofitel Raja Orchid Hotel, Khon Kaen, 18-20 October 2004, code AMM49.
- 3. Supasak, C. and Singhatanadgid, P. "A comparison of experimental buckling load of rectangular plates determined from various measurement methods," Proceedings of the 18th Conference of the Mechanical Engineering Network of Thailand (ME-NETT 18). Sofitel Raja Orchid Hotel, Khon Kaen, 18-20 October 2004, code AMM43.

Contents

Chapter 1. Introduction	1
Chapter 2. Literature review	5
2.1 Buckling of composite plate	5
2.2 Scaling law for buckling problem	9
Chapter 3. Scaling law applied to buckling problem	12
3.1 Similitude transformation	12
3.2 Scaling law for buckling of rectangular composite plates	13
3.3 Scaling law for buckling of annular orthotropic plates	16
Chapter 4. Theoretical verification.	
4.1 Buckling of rectangular plates	22
4.2 Buckling of polar orthotropic annular plates	24
4.3. Theoretical verification of rectangular plates	26
4.4 Theoretical verification of annular plates	30
Chapter 5. Experimental verification.	44
5.1 Experiment setup	44
5.2 Specimens and boundary conditions	45
5.3 Experiment procedures and data reduction	46
5.4 Scaling law verification	48
Chapter 6. Discussions and conclusions	61
References	64
Appendix	68

Chapter 1. Introduction

A so-called "advanced" composite material is a material system which consists of high strength and high modulus fibers embedded within a matrix material. Most of the loads applied to the composite structure are carried by fibers which are held together by the matrix. The matrix protects fibers from abrasion and transfers stresses from one fiber to the next. Because of their high strength-to-weight and stiffness-to-weight ratios, composite materials are extensively used in many applications in the aerospace, automotive, and marine industries. A main benefit of composite material is an ability to be tailored, which may not be obtained from conventional isotropic materials. Engineers can design the fiber orientations within the composite so that the desired mechanical properties are achieved.

In many applications, composites are manufactured in form of thin plate-like structures. Consequently, failure of laminated plates arises not only from excessive stresses but also from buckling. When a flat laminated plate is subjected to low in-plane compressive loads, the plate remains flat and is in equilibrium. As the magnitude of the in-plane compressive load increases, however, the equilibrium configuration of the plate is eventually changed to a non-flat configuration and the plate becomes unstable. The magnitude of the compressive load at which the plate becomes unstable is called the "critical buckling load" and at that level of load (or above) the panel is in a buckled condition. There are several studies in the past concerning the buckling problems of composite plates. Buckling behavior of composite plates has been determined using different approaches such as analytical methods, numerical methods, and experiment method. Each approach has its own advantages and disadvantages. Analytical approach is simple and straightforward for using in design of engineering structures since a closed

form solution is usually obtained. However, this method is limited to simple problems only, i.e. it cannot solve complicated problems. The numerical approaches such as the Ritz method, Galerkin method, and FEM are more versatile than the analytical method but they are time-consuming because of the intensive calculation. Although both methods may be used to predict the buckling behavior, however any new design usually requires extensive experiment evaluation before going to production. Experiment on a prototype is an ideal method for any new products since it is the best way to simulate every parameter's effect which might affect the specimen's behaviors. Then again, this method is very expensive and time consuming.

This is where the similitude method appears as an indispensable tool in order to be able to design efficient experiments to save time and cost. Similitude theory can be roughly stated to be a branch of science concerned with sufficient and necessary conditions of similarity among phenomena. If such similarity conditions can be found among parameters of the model and prototype, then the scaled replica can be built to duplicate the behaviors of the full-scaled system and the results from the model experiments can be employed to predict the behavior of the prototype which has complete similitude with the test model.

Simitses, et. al [1-4] have published several papers on cross-ply laminated plates that deal with the establishment of the similarity conditions between the two phenomena, the model and the prototype. Then they use these similarity conditions or "scaling laws" to design scaled-down models and employ the model data from theoretical calculation to predict the behavior of the prototypes from the scaling laws. However, they have applied the similitude theory to the solutions of the governing differential equations (GDE) instead of to the GDE directly. This procedure puts serious limitation on the applicability of the concept of similitude theory because some forms of exact or approximate analytical

solutions must be obtained before they can apply the similitude transformation. The main objective of this study is to derive the similitude invariants for buckling loads of the laminated composite plates subjected to in-plane loads by applying the similitude transformation to the governing differential equations directly. The derived similitude invariants are non-dimensional and applicable to both the models and the prototypes, hence "scaling laws" have been established. The validity of the scaling laws is then verified theoretically and experimentally. The buckling loads of the model and prototype are theoretically calculated from the available solutions. The theoretical results of the model are then substituted into the scaling laws to predict the buckling loads of the prototype. The results from the scaling law are finally compared with the theoretical solutions to determine the validity of the scaling law. Experimental verification is also employed by grouping specimens as models and prototypes before experimentally determine buckling of all specimens. Similar to the theoretical verification, buckling loads of the models are substituted into the scaling law to determine the similitude buckling loads of the prototypes. These similitude buckling loads are compared to the experimental buckling loads to determine the accuracy of the scaling law.

In summary, objectives of this study may be itemized as follows:

- 1. Derive scaling law for buckling of rectangular and annular composite plates from the governing differential equations
- 2. Verify the derived scaling law with the theoretical solutions
- 3. Perform an experiment on rectangular composite plates to verify the derived scaling law

In this report, buckling of composite plate and similitude theory are outlined and reviewed in the first two chapters. The discrepancy of experimental buckling load compared to the theoretical solution and the advantages of the similitude theory are pointed out. Similitude transformation is applied to buckling problem of rectangular composite plates and polar orthotropic annular plates in Chapter 3. The scaling laws for both problems and the similarity requirements are obtained. The obtained scaling laws are verified with available theoretical and numerical solutions in Chapter 4. The experimental verification was performed on rectangular composite plates and is described in Chapter 5. The experiment setup, testing procedure, and verification of the scaling law are explained, thoroughly. This report concludes in the last chapter with some discussions and conclusions of the present study and recommendations for future studies.

Chapter 2. Literature Review

This chapter gives a review of previous studies on buckling of anisotropic plates. The general buckling behaviors of thin plate are described in the first part of this chapter. Buckling behavior of flat composite plates is then reviewed with an emphasis on rectangular and annular composite plates. Both analytical and experimental studies that have appeared in the literatures are included. Finally, the similitude theory is reviewed in the last part of the chapter

2.1 Buckling of composite plate

Besides tensile or compression failures, buckling is another mode of failure that involves stability of structures. It usually happens in slender elements such as beams, columns, or plates. This study focuses on buckling of composite plates; so only plate structures are of interest herein. A panel subjected to uniaxial or biaxial compressive loading will buckle if compressive stress at any point is sufficiently high. A plate under compression-tension biaxial loading may also buckle. Buckling phenomenon may even arise from more complicated loading conditions such as non-uniform tensile loading, shear loading, moisture, or exposure to elevated temperatures.

The buckling phenomenon can be described from a plot of the out-of-plane displacement (w) at a specific point, usually at the point of maximum out-of-plane displacement, against in-plane load (P), as shown in Fig. 2.1. In classical linear buckling theory, when in-plane load (P) increases from zero, out-of-plane displacements are assured to remain zero, and a load-displacement curve follows Path I until load P_{cr} is reached. At this point, which is called a bifurcation point, the load-displacement curve

may follow Path II or Path III. If the in-plane load is perfectly applied at the mid-plane of a perfect plate, compressive failure of material could be reached by following Path II. There is no buckling in this case. Path III is a theoretical buckling path and can be obtained from classical linear buckling theory. The critical buckling load is defined on this horizontal line. In a nonlinear theory, the curve follows Path IV, the "postbuckling" curve. This curve is important in the study of plate behavior beyond the buckling load, P_{cr} . For a real plate with initial imperfections, the curve will not follow Path I, i.e. an out-of-plane displacement occurs as soon as load P is applied. In this case, the load-displacement curve will resemble Path V.

Although laminated composite plates have been successfully used in a wide range of applications, a complete understanding of the mechanical behavior exhibited by composites has not been accomplished, and new research results appear continuously. Studies concerning anisotropic plates began to appear in the 1950's and early 1960's. A textbook devoted to mechanics of anisotropic plate by Lekhnitskii [5] appeared in 1956. These early publications lay the foundation for later studies of the bending, buckling, and vibration of composite plates, which began to appear with increasing frequency in the late 1960's.

There are several texts devoted to buckling of composite plates and very well-known to researchers. A text book by Whitney [6] published in 1987 covers several topics from mechanics of composite material to analysis of anisotropic structures. The buckling problem of composite plates also appears in several textbooks devoted to fundamental mechanics of composite [7-9]. A textbook by Turvey and Marshall [10] released in 1995 devotes specifically to buckling and postbuckling of composite plates. This book covers several methods used in buckling analysis such as the Ritz method, finite element analysis, and finite strip method. Besides several available textbooks, summaries of

advanced topics and recent developments in laminated plates are appeared in the review papers by Leissa [11,12], and Kapania *et al.* [13].

Buckling of composite plates can be investigated using analytical and numerical analysis. Analytical solution of the buckling of composite plates requires a solution of the governing equations. These equations are only solvable in a few simple cases, such as a specially orthotropic rectangular plate with simply supported boundary conditions. In more general problems an analytical closed form solution is generally not available, primarily due to the bending-twisting coupling terms, D_{16} and D_{26} . In these cases a numerical method, usually based on an energy principle, is employed to obtain an approximate solution. The Ritz and Galerkin methods are two common techniques used to obtain the solutions approximately. These approximation techniques can be performed easily and give reasonable results with minimal computational efforts; that is, these methods are less computationally intense than another numerical method, the finite element technique. The finite element method is based on either an incremental approach or asymptotic method. It enables an engineer to solve plate problems with complex geometry, complicated boundary condition, or even nonlinear problem. However, lengthy calculations are involved in this approach. Although a modern computation tools such as supercomputers are now available, the versatility of finite element analysis is still somewhat restricted by computation time and memory needed, at least during the preliminary design process.

A closed-form solution for a specially orthotropic plate, i.e. either unidirectional or a symmetric cross-ply panels, is thoroughly derived by Whitney [6]. Mode shape transitions are also graphically presented. Several studies on buckling of composite plates using the Ritz method are available. In 1986, Lagace *et al.* [14] employed the Ritz method to study the effect of mechanical couplings on buckling behavior. They concluded that

those mechanical couplings, especially stretching-bending couplings, cause out-of-plane displacement prior to buckling in unsymmetric laminates. This phenomenon significantly reduces the critical buckling load. An experimental verification was also performed. The Ritz method was demonstrated, by Narita and Leissa [15], to be accurate for symmetric laminates if enough number of terms (more than 100 terms) were used. A double sine series was used to approximate the out-of-plane displacement. Convergence studies and contour plots of buckling mode shape were also presented. However, the in-plane displacements were ignored in the strain energy function. Similar approximate function and analysis method were used by Chai and Hoon [16] to study the buckling of generally laminated plates. The results agreed with the exact solution for symmetric crossply, antisymmetric crossply, and antisymmetric angle-ply. The effect of mechanical couplings, D_{16} and D_{26} , on buckling load was shown to be an important factor in the analysis.

Buckling studies of composite plates have not only been limited to simple rectangular plates, but irregular plates such as elliptical plates, triangular plates, or annular plates have also been explored. Ramaiah [17] used the Rayleigh-Ritz method to determine the critical buckling load of polar orthotropic annular plates with various load ratios and rigidity ratios. The numerical solutions in form of buckling load parameters are tabulated for direct used in design process. Doki and Tani [18] studied the buckling of similar annular plates under a combination of internal radial pressure and torsion using the Galerkin method. Asymmetric buckling modes were also considered in addition to axisymmetric buckling mode. Besides buckling load, buckling mode is also investigated. There are several other researches which are relevant to the present study. For example, Ye [19] studied axisymmetric buckling of laminated annular plate by considering the problem as a fully three-dimensional elasticity problem. Buckling of moderately thick polar orthotropic annular plates was investigated by Chang [20]. Dumar et al.[21]

included the shear deformation theory to study the postbuckling of thick laminated annular plates.

There have been several experimental studies on buckling of composite plates using different measurement techniques appeared during the past two decades. Chai, Hoon, and Chin [22] experimentally confirmed the buckling behavior determined from the Ritz method using laser-based holography and strain gauges. Chai, Banks, and Rhodes [23] used a linear variable differential transformer (LVDT) to measure the out-ofplane deflection to study the buckling of simply supported plates under uniaxial loading. The results correlated well with finite element solutions and other available studies [24,25]. Discrepancies between -7% and 11% of experimentally determined buckling loads were reported. Another experimental method for monitoring out-of-plane displacement is the shadow moiré technique. This experiment method was used by Tuttle, Singhatanadgid, and Hinds [26] to observe the whole-field out-of-plane deflections of composite plates under tension-compression biaxial loading. Experimental buckling modes were well compared with predictions obtained numerically based on the Galerkin method. As expected, buckling loads increased as the transverse tensile loads were increased. Almost all of the previous studies indicated several difficulties in setting up the experimental conditions, such as loading conditions and boundary conditions, which are comparable to the conditions assumed in the analysis. These factors are the common sources of discrepancy between measurement and prediction.

2.2 Scaling law for buckling problem

From a brief literature review in the previous section, buckling problems of composite plates can be examined using a variety of approaches. Each method has

advantages and disadvantages. The analytical approach is the simplest method to determine buckling load and mode, but it is applicable to only a group of problems. The semi-analytical-numerical methods such as the Ritz and Galerkin methods are more general and capable to solve problems which do not have a closed-form solution. Certainly, these methods required more calculation than the analytical approach. The last approaches are the fully numerical method which is the most powerful, but requires the most resources compared to other methods. This calculation category includes finite element, finite strip, and boundary element methods. Although there are several analytical and numerical methods available, several experimental studies have also been performed. The percent discrepancy of $\pm 20\%$ between experiment results and available analytical or numerical solutions is usually reported. The likely sources of discrepancy are imperfections of the specimen and boundary conditions. To be specific, the prediction of buckling load and mode using available approaches is not accurate because the imperfections of the real structure are not included in the mathematical model. There is a need to predict the buckling of composite plate containing imperfections.

Rezaeepazhand, et. al [3] employed similitude theory to buckling of laminated composite plate problems. The scaling laws shown the relationship between buckling load of a prototype structure and its models were obtained. Rezaeepazhand, et. al [27] also applied similitude theory to the free vibration of laminated plates. The relationship between structural geometric parameters and frequency parameters were obtained from the scaling laws. Both cross-ply and angle-ply symmetric plates were included in the study. The similar approach was also employed to bending, buckling, and vibration of flat laminated surfaces by Simitses [28]. In the similitude studies mentioned so far, the authors have applied the similitude transformation to the solutions of the governing differential equations instead of to the governing differential equations directly. This

procedure puts serious limitation on the applicability of the concept of similitude theory because some forms of exact or approximate analytical solutions must be obtained before they can apply the similitude transformation. Singhatanadgid *et. al* [29] and Ungbhakorn *et. al* [30] proposed a new similitude approach which applies the similitude transformation to the buckling governing differential equations directly. They showed numerically that the buckling loads of the model and the prototype are related via the scaling law if the model-prototype pair has complete similarity.

In this study, the scaling laws for buckling of rectangular cross-ply plates derived by Singhatandgid *et. al* [29] were experimentally verified. The composite specimens were classified into two groups, i.e. model and prototype. Both specimens were tested on a compression test frame for buckling loads which were then used to verify the derived scaling laws. The similitude transformation was also applied to a more complicated buckling problem, i.e. buckling of polar orthotropic annular plates.

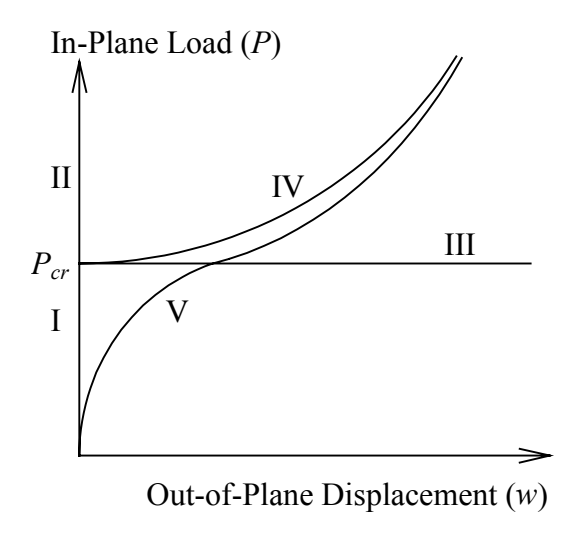


Fig. 2.1 Buckling phenomenon represented by a plot of P vs. w

Chapter 3. Scaling law applied to buckling problem

In this chapter, similitude theory is applied to buckling of composite plate problems. The similitude theory and similitude invariant are first illustrated by applying the similitude transformation to the governing equations. The concept is then applied to buckling of rectangular plate and annular plate problems. The similitude invariants and scaling laws are obtained for both problems. Both scaling laws are verified analytically and experimentally in the next chapters.

3.1 Similitude transformation

Similitude theory is extensively described in a few textbooks [31-33]. Only a brief summary which is relevant to this study will be presented as follows. The essence of similitude theorem relevant to this research can be stated as: the sufficient and necessary condition of similitude between two systems is that the mathematical model of the one be related by a bi-unique transformation to that of the other [33]. The two systems refer to a model and a prototype. Usually, the prototype is the system of the real structure which is not convenient or too expensive to conduct an experiment on. The model system is a replica of the prototype with particular scaling factors. Thus, this system can be resized to fit the experiment setup and budget. Considering all variables, geometric and physical, of the prototype and the model denoted by X_{pi} and X_{mi} respectively, where i = 1, 2, ... n. The two systems or phenomena are similar if

$$X_p = CX_m$$
 and $X_m = C^{-1} X_p$

Since the mathematical models of two similar systems are invariable under similar systems, therefore similar systems are invariable under similar systems.

$$L(X_{mi}) = L(X_{pi}) (3.1)$$

Let the model and prototype variables be related to each other by the equations:

$$X_{pi} = C_i X_{mi} ag{3.2}$$

Substitute eq(3.2) into (3.1), the relation yields

$$L(X_{mi}) = L(C_i X_{mi}) \tag{3.3}$$

From the above theorem, it is necessary that

$$L(X_{mi}) = \varphi(C_i) L(X_{mi}) \tag{3.4}$$

where $\varphi(C_i)$ is the functional relationship among the transformation parameters. If both systems have similarity according to the similarity conditions, it is compulsory that

$$\varphi(C_i) = 1 \tag{3.5}$$

Hence, the condition for the two systems to be similar is that the function linking the transformation parameters equals to unity. The equation $\varphi(C_i) = 1$, is accordingly called the similar invariant. From the similar invariant, the scaling law relating a particular parameter of both systems can be derived. Next, this similar concept is applied to buckling problems of rectangular plates and polar orthotropic annular plates.

3.2 Scaling law for buckling of rectangular composite plates

The similitude theory will be applied to the governing differential equation for buckling of the symmetrically laminated plates subjected to combined normal in-plane loads. A rectangular composite plate is loaded in the x and y directions as shown in Fig 3.1. The transverse tensile load N_{yy} is related to the compressive load N_{xx} by the in-plane load ratio defined by $P = \frac{N_{yy}}{N_{xx}}$. The specimen is buckled due to the compressive load in

the x direction. The classical buckling differential equation is simplified to [6]

$$D_{11}w_{,xxxx} + 4D_{16}w_{,xxxy} + 2(D_{12} + 2D_{66})w_{,xxyy} + 4D_{26}w_{,xyyy} + D_{22}w_{,yyyy} + N_{xx}(w_{,xx} + Pw_{,yy}) = 0$$
(3.6)

Let the variables of the prototype be related to those of the model through the similitude scaling factors $(C_x, C_y, C_{w...})$ as follows.

$$x_{p} = C_{x}x_{m}, \quad y_{p} = C_{y}y_{m}, \quad w_{p} = C_{w}w_{m},$$

$$(D_{ij})_{p} = C_{Dij}(D_{ij})_{m}, \quad P_{p} = C_{p}P_{m}, \quad \text{and} \quad (N_{xx})_{p} = C_{Nxx}(N_{xx})_{m}$$
(3.7)

where subscripted "p" refers to "prototype" and subscripted "m" refers to "model"

The governing equation for a model can be written from eq(3.6) with a subscript "m" for every parameter. The equation for the model is;

$$(D_{11})_{m} (w_{,xxxx})_{m} + 4(D_{16})_{m} (w_{,xxxy})_{m} + 2\{(D_{12})_{m} + 2(D_{66})_{m}\}(w_{,xxyy})_{m}$$

$$+ 4(D_{26})_{m} (w_{,xyyy})_{m} + D_{22} (w_{,yyyy})_{m} + (N_{xx})_{m} \{(w_{,xx})_{m} + P_{m} (w_{,yy})_{m}\} = 0$$

$$(3.8)$$

Similarly, the governing equation for the prototype can be represented by an equation similar to eq(3.8), only substituting the subscript "m" with subscript "p." This governing equation can be written in term of the parameters of the model using the scaling factors in eq(3.7). The equation is represented by

$$C_{D11} \frac{C_{w}}{C_{x}^{4}} (D_{11})_{m} (w_{,xxxx})_{m} + 4C_{D16} \frac{C_{w}}{C_{x}^{3} C_{y}} (D_{16})_{m} (w_{,xxxy})_{m}$$

$$+2 \left\{ C_{D12} (D_{12})_{m} + 2C_{D66} (D_{66})_{m} \right\} \frac{C_{w}}{C_{x}^{2} C_{y}^{2}} (w_{,xxyy})_{m}$$

$$+4C_{D26} \frac{C_{w}}{C_{x} C_{y}^{3}} (D_{26})_{m} (w_{,xyyy})_{m} + C_{D22} \frac{C_{w}}{C_{y}^{4}} D_{22} (w_{,yyyy})_{m}$$

$$+C_{Nxx} (N_{xx})_{m} \left\{ \frac{C_{w}}{C_{x}^{2}} (w_{,xx})_{m} + C_{P} \frac{C_{w}}{C_{y}^{2}} P_{m} (w_{,yy})_{m} \right\} = 0$$

$$(3.9)$$

The governing equations of the model and the prototype are similar if all groups of the scaling factors in each term of the prototype's governing equation are identical. The following necessary conditions for the models to behave exactly as the prototype are obtained:

$$\frac{C_{D11}}{C_x^4} = \frac{C_{D16}}{C_x^3 C_y} = \frac{C_{D12}}{C_x^2 C_y^2} = \frac{C_{D66}}{C_x^2 C_y^2} = \frac{C_{D26}}{C_x C_y^3} = \frac{C_{D22}}{C_y^4} = \frac{C_{Nxx}}{C_x^2} = \frac{C_{Nxx} C_P}{C_y^2}$$
(3.10)

Let the prototype and model be related with complete geometric similarity, therefore $C_x = C_y = C_a = C_b$, where a and b are plate height and width, respectively. Thus, eq(3.10) is true only if C_P equals to unity, hence, it can be rewritten as:

$$C_{Nxx} = \frac{C_{D11}}{C_h^2} = \frac{C_{D16}}{C_h^2} = \frac{C_{D12}}{C_h^2} = \frac{C_{D66}}{C_h^2} = \frac{C_{D26}}{C_h^2} = \frac{C_{D22}}{C_h^2}$$
(3.11)

For complete similarity between the prototype and its model, it is required that the scaling factors of all laminate flexural stiffnesses must be equal, i.e.

$$C_{D11} = C_{D16} = C_{D12} = C_{D22} = C_{D26} = C_{D66}$$
(3.12)

Let the scaling factors of the flexural stiffnesses be equal to C_{stiff} , then the above equations yield the following similitude invariant for the symmetric laminated plates subjected to combined in-plane loads:

$$\frac{C_{Nxx}C_b^2}{C_{stiff}} = 1 \tag{3.13}$$

which gives the following scaling law:

$$(N_{xx})_p = (N_{xx})_m C_{stiff} \frac{b_m^2}{b_p^2}$$
 (3.14)

The derived scaling law is valid for both symmetric cross-ply and angle-ply laminates. For cross-ply laminated plates, the complete similitude requirement of the stiffness scaling factor in eq(3.12) is simplified by excluding the terms containing C_{D16} and C_{D26} because those stiffnesses are zero automatically. In conclusion, the complete similitude is achieved when the prototype and model have complete geometric similarity, that is $C_a = C_b$ and they are subjected to the same load ratio, $C_P = 1$. It is also required that the scaling factors of all non-zero laminate flexural stiffnesses must be equal.

3.3 Scaling law for buckling of annular orthotropic plates

In this section, the similitude transformation is applied to a more complicated buckling problem, i.e. a buckling problem of polar orthotropic annular plates. A thin annular plate of uniform thickness h is composed of a polar orthotropic material with inner and outer radii of a and b, respectively. The plate is clamped on both internal and external edges. Two cases of buckling conditions considered in this study are in-plane radial compressive loads, P_i and P_o , and torsional shearing load of Q_s and $Q_s \left(\frac{b}{a}\right)^2$, as shown in Fig 3.2. The buckling governing equation for both cases is [18]

$$D_{r}w_{,rrrr} + \frac{2D_{r}}{r}w_{,rrr} - \frac{D_{\theta}}{r^{2}}w_{,rr} + \frac{D_{\theta}}{r^{3}}w_{,r} - \frac{2}{r^{3}}(D_{1} + D_{r\theta})w_{,r\theta\theta} + \frac{2}{r^{2}}(D_{1} + D_{r\theta})w_{,rr\theta\theta} + \frac{2}{r^{4}}(D_{\theta} + D_{1} + D_{r})w_{,\theta\theta} + \frac{D_{\theta}}{r^{4}}w_{,\theta\theta\theta\theta} -N_{r}^{o}w_{,rr} - N_{\theta}^{o} \cdot \left(\frac{1}{r}w_{,r} + \frac{1}{r^{2}}w_{,\theta\theta}\right) - 2Q_{s}\left(\frac{b}{r}\right)^{2}\left(\frac{w_{,r\theta}}{r} - \frac{w_{,\theta}}{r^{2}}\right) = 0$$
(3.15)

where
$$N_r^o = h(P \cdot r^{k-1} + Q \cdot r^{-k-1})$$

$$N_{\theta}^{o} = hk\left(P \cdot r^{k-1} - Q \cdot r^{-k-1}\right)$$

$$P = \frac{-\left(P_o b^{k+1} - P_i a^{k+1}\right)}{b^{2k} - a^{2k}} = \frac{-P_o \left(b^{k+1} - q a^{k+1}\right)}{b^{2k} - a^{2k}}$$

$$Q = \frac{\left(P_o a^{k-1} - P_i b^{k-1}\right) \cdot \left(ab\right)^{k+1}}{b^{2k} - a^{2k}} = \frac{P_o \left(a^{k-1} - q b^{k-1}\right) \cdot \left(ab\right)^{k+1}}{b^{2k} - a^{2k}}$$

$$D_{r} = \frac{E_{r}h^{3}}{12(1 - v_{r}v_{\theta})}, \qquad D_{\theta} = \frac{E_{\theta}h^{3}}{12(1 - v_{r}v_{\theta})}, \qquad D_{r\theta} = \frac{Gh^{3}}{6}, \quad D_{1} = v_{\theta}D_{r} = v_{r}D_{\theta}$$

For buckling caused by radial compressive load only, the torsional shearing load Q_s shown in eq(3.15) vanishes. Similarly, radial compressive loads are zero for the case of torsional buckling only, i.e. N_r^o and N_θ^o are absent from the governing equation.

Now, the similitude transformation is applied to the governing equation, eq(3.15). Let call two systems of interest a "model" and a "prototype" and let the parameters of the model be related to those of the prototype through the similitude scaling factors as follows:

$$\theta_{p} = \theta_{m}, \ r_{p} = C_{r} r_{m}, \ w_{p} = C_{w} w_{m}, \ h_{p} = C_{h} h_{m}, \ q_{p} = C_{q} q_{m},$$

$$(P_{o})_{p} = C_{Po} (P_{o})_{m}, \ (D_{r})_{p} = C_{Dr} (D_{r})_{m}, \ (D_{\theta})_{p} = C_{D\theta} (D_{\theta})_{m},$$

$$(D_{r\theta})_{p} = C_{Dr\theta} (D_{r\theta})_{m}, \ (D_{1})_{p} = C_{D1} (D_{1})_{m}, \ \text{and} \ k_{p} = C_{k} k_{m} = k_{m}$$

$$(3.16)$$

where C_i is the scaling factor of the i parameter, and $C_k = \left(\frac{C_{D\theta}}{C_{Dr}}\right)^{\frac{1}{2}}$ according to the definition of k. It should be noted that coordinates θ of the model and the prototype are identical or the scaling factor of θ is 1. In addition, the scaling factor C_k which is equal to $\left(\frac{C_{D\theta}}{C_{Dr}}\right)^{\frac{1}{2}}$ is also set to be unity. This implies that $C_{D\theta} = C_{Dr}$ which will be shown later that this is the condition for complete similitude.

The similitude transformation can be accomplished by writing the governing equations for the model and the prototype. The governing equation of the model is written from eq(3.15) by substituting the variables N_r^o and N_θ^o with the appropriated values shown previously. Most of the parameters are subscripted by "m" to indicate that the equation is the governing equation of the model. The only two non-subscripted parameters are θ and k, since they are set to be identical for both systems. For example, the first four terms of the governing equation of the model can be written as:

$$(D_r)_m \frac{\partial^4 w_m}{\partial r_m^4} + \frac{2(D_r)_m}{r_m} \frac{\partial^3 w_m}{\partial r_m^3} - \frac{(D_\theta)_m}{r_m^2} \frac{\partial^2 w_m}{\partial r_m^2} + \frac{(D_\theta)_m}{r_m^3} \frac{\partial w_m}{\partial r_m} - \dots = 0$$
 (3.17)

The governing equation for the prototype can be written in term of the model parameters by substituting appropriate similarity scaling factors from eq(3.16). Again, the first four terms of the equation are written as

$$C_{Dr} \frac{C_{w}}{C_{r}^{4}} (D_{r})_{m} \frac{\partial^{4} w_{m}}{\partial r_{m}^{4}} + \frac{C_{Dr}}{C_{r}} \frac{C_{w}}{C_{r}^{3}} \frac{2(D_{r})_{m}}{r_{m}} \frac{\partial^{3} w_{m}}{\partial r_{m}^{3}} - \frac{C_{D\theta}}{C_{r}^{2}} \frac{C_{w}}{C_{r}^{2}} \frac{(D_{\theta})_{m}}{r_{m}^{2}} \frac{\partial^{2} w_{m}}{\partial r_{m}^{2}} + \frac{C_{D\theta}}{C_{r}^{3}} \frac{C_{w}}{C_{r}^{2}} \frac{(D_{\theta})_{m}}{r_{m}^{3}} \frac{\partial w_{m}}{\partial r_{m}} \dots = 0$$
(3.18)

To obtain the similarity between both systems according to the similarity concept, governing equations for the model and prototype, eq(3.17) and eq(3.18), must be identical. Specifically, groups of scaling factors in each term of the eq(3.18) must be equal so that they are canceled out. Thus, the requirements of similarity or conditional equations for both systems to behave similarly are:

$$C_{Dr} \frac{C_{w}}{C_{r}^{4}} = \frac{C_{Dr}}{C_{r}} \frac{C_{w}}{C_{r}^{3}} = \frac{C_{D\theta}}{C_{r}^{2}} \frac{C_{w}}{C_{r}^{2}} = \frac{C_{D\theta}}{C_{r}^{3}} \frac{C_{w}}{C_{r}} = \frac{C_{D1}}{C_{r}^{3}} \frac{C_{w}}{C_{r}} = \frac{C_{Dr\theta}}{C_{r}^{3}} \frac{C_{w}}{C_{r}}$$

$$= \frac{C_{D1}}{C_{r}^{2}} \frac{C_{w}}{C_{r}^{2}} = \frac{C_{Dr\theta}}{C_{r}^{2}} \frac{C_{w}}{C_{r}^{2}} = \frac{C_{D\theta}}{C_{r}^{4}} C_{w} = \frac{C_{D1}}{C_{r}^{4}} C_{w} = \frac{C_{Dr}}{C_{r}^{4}} C_{w} = \frac{C_{D\theta}}{C_{r}^{4}} C_{w}$$

$$= C_{h} C_{po} C_{r}^{k-1} \frac{C_{b}^{k+1}}{C_{b}^{2k}} \frac{C_{w}}{C_{r}^{2}} = C_{h} C_{po} C_{r}^{k-1} \frac{C_{q} C_{b}^{k+1}}{C_{b}^{2k}} \frac{C_{w}}{C_{r}^{2}} = C_{h} C_{po} C_{b}^{2k+2} C_{r}^{-k-1} \frac{C_{b}^{k-1}}{C_{b}^{2k}} \frac{C_{w}}{C_{r}^{2}}$$

$$= C_{h} C_{po} C_{b}^{2k+2} C_{r}^{-k-1} \frac{C_{q} C_{b}^{k-1}}{C_{b}^{2k}} \frac{C_{w}}{C_{r}^{2}} = C_{h} C_{po} C_{r}^{2k+2} C_{r}^{-k-1} \frac{C_{q} C_{b}^{k+1}}{C_{b}^{2k}} \frac{C_{w}}{C_{r}^{2}}$$

$$= C_{h} C_{po} C_{b}^{2k+2} C_{r}^{-k-1} \frac{C_{b}^{k-1}}{C_{b}^{2k}} \frac{C_{w}}{C_{r}^{2}} = C_{h} C_{po} C_{b}^{2k+2} C_{r}^{-k-1} \frac{C_{q} C_{b}^{k-1}}{C_{b}^{2k}} \frac{C_{w}}{C_{r}^{2}}$$

$$= C_{h} C_{po} C_{b}^{2k+2} C_{r}^{-k-1} \frac{C_{b}^{k-1}}{C_{b}^{2k}} \frac{C_{w}}{C_{r}^{2}} = C_{h} C_{po} C_{b}^{2k+2} C_{r}^{-k-1} \frac{C_{q} C_{b}^{k-1}}{C_{b}^{2k}} \frac{C_{w}}{C_{r}^{2}}$$

$$= C_{h} C_{po} C_{b}^{2k+2} C_{r}^{-k-1} \frac{C_{b}^{k-1}}{C_{b}^{2k}} \frac{C_{w}}{C_{r}^{2}} = C_{h} C_{po} C_{b}^{2k+2} C_{r}^{-k-1} \frac{C_{q} C_{b}^{k-1}}{C_{b}^{2k}} \frac{C_{w}}{C_{r}^{2}}$$

$$= C_{h} C_{po} C_{b}^{2k+2} C_{r}^{-k-1} \frac{C_{b}^{k-1}}{C_{b}^{2k}} \frac{C_{w}}{C_{r}^{2}} = C_{h} C_{po} C_{b}^{2k+2} C_{r}^{-k-1} \frac{C_{q} C_{b}^{k-1}}{C_{b}^{2k}} \frac{C_{w}}{C_{r}^{2}}$$

Note that the geometric similarity is assumed in the similarity requirements so that C_r , C_a and C_b are identical and represented by C_b . It is further assumed that the load ratio of both systems are identical, i.e. $C_q = 1$. Therefore, the similarity requirements in eq(3.19) are simplified as:

$$\frac{C_{Dr}}{C_b^4} = \frac{C_{D\theta}}{C_b^4} = \frac{C_{D1}}{C_b^4} = \frac{C_{Dr\theta}}{C_b^4} = \frac{C_h C_{Po}}{C_b^2} = \frac{C_{Qs}}{C_b^2}$$
(3.20)

which imply that $C_{Dr} = C_{D\theta} = C_{D1} = C_{Dr\theta}$ for complete similitude.

In summary, the requirements for complete similarity between the model and the prototype include a) the complete geometric similarity, b) identical load ratio q and rigidity ratio k, and c) identical stiffness scaling factors. By representing all of the stiffness scaling factors by C_{stiff} , eq(3.20) can be rearranged in term of similarity invariant for the buckling problem caused by internal and external compressive loads as:

$$\frac{C_h C_{Po} C_b^2}{C_{stiff}} = 1 \tag{3.21}$$

The scaling law for buckling of polar orthotropic annulus plates under internal and external compressive loads is then obtained as:

$$\left(P_{o}\right)_{p} = C_{stiff} \frac{h_{m}}{h_{p}} \frac{b_{m}^{2}}{b_{p}^{2}} \left(P_{o}\right)_{m} \tag{3.22}$$

For buckling caused by torsional shear load, the similitude invariant and the scaling law are written as:

$$\frac{C_{Qs}C_b^2}{C_{stiff}} = 1 \tag{3.23}$$

and
$$(Q_s)_p = C_{stiff} \frac{b_m^2}{b_p^2} (Q_s)_m$$
 (3.24)

It is notice that the scaling laws derived for both buckling cases are independent of the plate boundary conditions. It implies that the scaling law can be used to predict the behavior of the prototype, provided that both model and prototype have the same boundary conditions and all the similarity requirements are satisfied.

In conclusion, similitude transformation is employed to buckling problems of composite plates. Both symmetrical rectangular plates and polar orthotropic plates are included in this study. Along with the scaling laws, the conditions for complete similarity between two systems are also obtained. The derived scaling laws, i.e. eq(3.14), eq(3.22), and eq(3.24), will be verified in the next two chapters. In chapter 4, the derived scaling laws are verified using available analytical or numerical solutions. The buckling loads and modes of prototypes are determined from the available solutions. They are then compared to those of determined from the scaling laws which are calculated using

buckling load of the corresponding models. The experimental verification of rectangular specimens is presented in chapter 5.

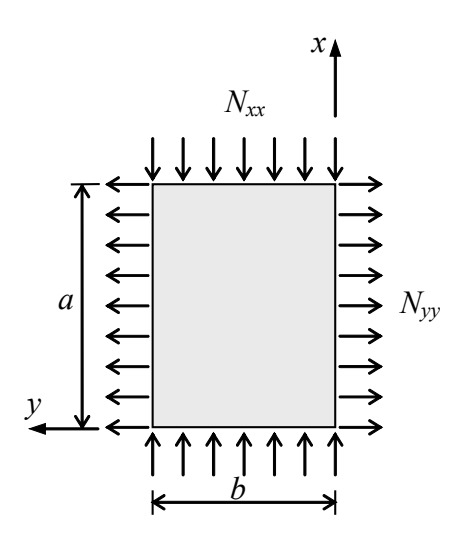


Fig 3.1 Rectangular plate subjected to in-plane load N_{xx} , and N_{yy}

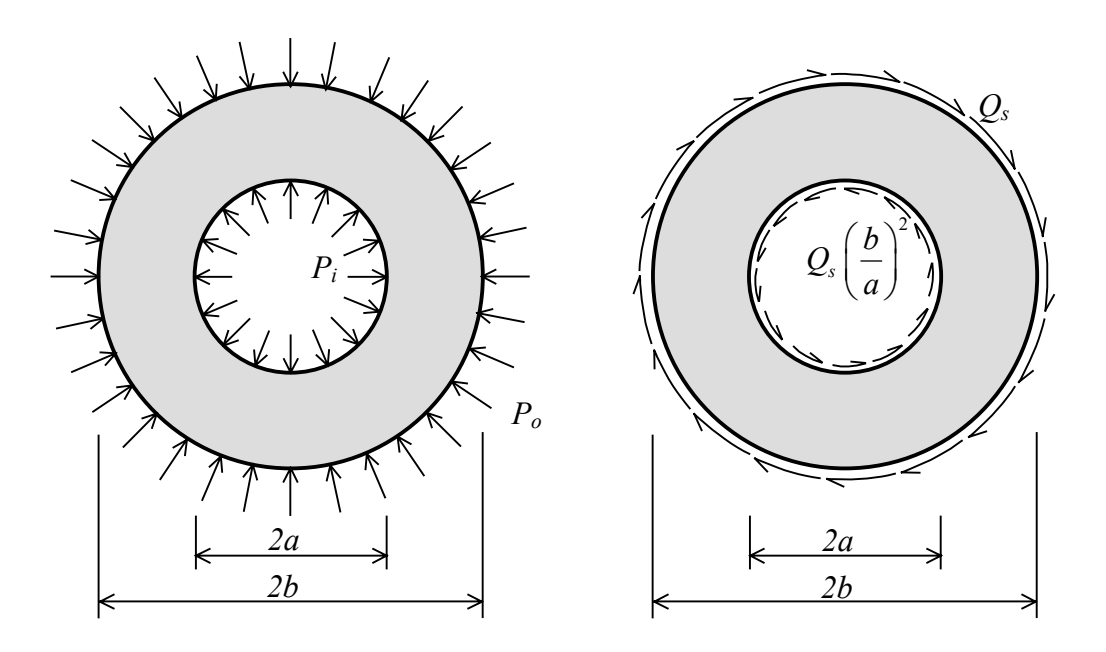


Fig. 3.2. Annular plate under compressive radial and torsional loading

Chapter 4. Theoretical Verification

The scaling laws for both buckling problems are derived in the previous chapter along with their similarity requirements. In this chapter, the derived scaling law will be verified with the theoretical or numerical solutions. The buckling solutions for symmetrical rectangular plates and polar orthotropic annular plates are outlined in the first two sections. Then, the accuracy of the scaling law is determined using available solutions. Both complete and partial similitude cases are investigated.

4.1 Buckling of rectangular plates

For the case of symmetric cross-ply laminated plates subjected to biaxial loading, as shown in Fig 3.1, with classical simply-supported boundary condition the buckling load can be derived from the governing equation, eq(3.1) as [6]

$$N_{xx} = \frac{\pi^2 \left[D_{11} \left(\frac{m}{a} \right)^4 + 2 \left(D_{12} + 2 D_{66} \right) \left(\frac{mn}{ab} \right)^2 + D_{22} \left(\frac{n}{b} \right)^4 \right]}{\left[\left(\frac{m}{a} \right)^2 + P \left(\frac{n}{b} \right)^2 \right]}$$
(4.1)

But due to terms with odd number of derivatives in the governing equation, the solution for symmetric angle-ply laminated plates subjected to biaxial loading with simply-supported boundary condition will be calculated from an approximate solution by the Ritz method [6].

The Ritz method begins with selecting the mid-plane displacement functions which satisfy the geometrical boundary conditions. In case of a simply supported plate the out-of-plane displacement is approximated in form of a double sine series as

$$w(x,y) = \sum_{m=1}^{M} \sum_{n=1}^{N} A_{mn} \sin\left(\frac{m\pi x}{a}\right) \sin\left(\frac{n\pi y}{b}\right)$$
(4.2)

where A_{mn} are unknown coefficients to be determined, M and N indicate numbers of terms used in the series. This approximate function is then used to calculate the total potential energy of a plate subjected to in-plane loading. The total potential energy (Π) can be written in term of the sum of strain energy (U) and potential energy of in-plane loads (V)

$$\Pi = U + V \tag{4.3}$$

where

$$U = \frac{1}{2} \iiint \left(\sigma_{xx} \varepsilon_{xx} + \sigma_{yy} \varepsilon_{yy} + \sigma_{xy} \gamma_{xy} \right) dx dy dz$$

$$V = \frac{1}{2} \iint \left\{ N_{xx} \left(\frac{\partial w}{\partial x} \right)^2 + N_{yy} \left(\frac{\partial w}{\partial y} \right)^2 + 2N_{xy} \frac{\partial w}{\partial x} \frac{\partial w}{\partial y} \right\} dx dy$$

After performing the integrations the total potential energy can be written in terms of the unknown coefficients A_{mn} and the in-plane normal load N_{xx} . Other in-plane loads, i.e. N_{yy} and N_{xy} , can prescribe as the multiplication of N_{xx} and load ratio. According to the minimum total potential energy:

$$\frac{\partial \Pi}{\partial A_{mn}} = 0 \tag{4.4}$$

A set of equations may be rearranged in a form of an eigenvalue problem as

$$[A][C] - N_{xx}[B][C] = 0 (4.5)$$

where [A] and [B] are square matrices whose elements are determined from the plate properties. [C] is a column matrix containing unknown eigenvectors, A_{mn} . N_{xx} represents the unknown eigenvalue or the buckling load.

A number of eigenvalues will be obtained after the generalized eigenvalue problem shown in eq(4.5) is solved. The lowest eigenvalue is selected as the buckling load. The corresponding eigenvector representing the buckling mode, however, is not of interest in this study.

4.2 Buckling of polar orthotropic annular plates

For polar orthotropic annular plates, either closed-form solutions or experimental results are not available due to the orthotropic property of material. Therefore, the Ritz method is employed to determine the numerical solution. The Ritz method begins with selecting the mid-plane displacement functions which satisfy the geometrical boundary conditions. In case of a clamped annular plate, the out-of-plane displacement which satisfies all boundary conditions is approximated in form of a trigonometric series as

$$w(r,\theta) = \left(\frac{r}{a} - 1\right)^2 \left(\frac{r}{b} - 1\right)^2 \sum_{m=0}^{M} r^m \left(A_m \sin n\theta + B_m \cos n\theta\right)$$
(4.6)

where A_m and B_m are unknown coefficients to be determined, n is a positive integer indicating the number of full sine wave in the circumferential direction. The integer n also indicates the buckling mode of the plate. Theoretically, it is desirable to have as many terms as possible in the approximate function, i.e. M approaches infinity, however only a number of terms are used due to the numerical limitation. This approximate function is then used to calculate the total potential energy of a plate subjected to in-plane loads. The total potential energy (Π) can be written in term of the sum of strain energy (U) and potential energy due to in-plane loads (V), as represent in eq(4.3), where

$$U = \frac{1}{2} \int_{0}^{2\pi} \int_{a}^{b} \left\{ D_{r} \left[w_{,rr} \right]^{2} + 2D_{1} w_{,rr} \left(\frac{1}{r^{2}} w_{,\theta\theta} + \frac{1}{r} w_{,r} \right) + D_{\theta} \left(\frac{1}{r^{2}} w_{,\theta\theta} + \frac{1}{r} w_{,r} \right)^{2} + 2D_{r\theta} \left[\left(\frac{1}{r} w_{,\theta} \right)_{,r} \right]^{2} \right\} r dr d\theta$$

$$(4.7)$$

$$V = \frac{1}{2} \int_{0}^{2\pi} \int_{a}^{b} \left\{ N_{r}^{o} r \left[w_{,r} \right]^{2} + \frac{N_{\theta}^{o}}{r} \left[w_{,\theta} \right]^{2} + \frac{2Q_{s}b^{2}}{r^{2}} w_{,r} w_{,\theta} \right\} dr d\theta \tag{4.8}$$

After substituting the approximate displacement function and performing the integrations, the total potential energy can be written in terms of the unknown coefficients A_m , B_m , and the applied load. In case of buckling from radial compressive load, the applied load is the in-plane radial load P_o , while Q_s is the applied load for torsional buckling. According to the concept of minimum total potential energy, the structure is in stable equilibrium if

$$\frac{\partial \Pi}{\partial A_m} = 0$$
 and $\frac{\partial \Pi}{\partial B_m} = 0$ (4.9)

A convergence study on buckling of graphite-epoxy annular plate with a=50 mm, b=200 mm, h=2 mm and a load ratio of 0.5 was performed. Both compressive and torsional buckling loads are plotted as a function of M used in the approximate function as shown in Fig. 4.1. The buckling load is conversed to the theoretical value as the value of M is increased. In this study, the value of M in the approximate function $w(r,\theta)$ are selected as 6, so eq(4.9) is a set of 14 linear functions. The set of equations may be rearranged in a form of a generalized eigenvalue problem as

$$[A][C] - L[B][C] = 0$$
 (4.10)

where [A] and [B] are square matrices whose elements are determined from plate dimensions and material properties. [C] is a column matrix containing unknown eigenvectors, A_m and B_m . L represents the unknown eigenvalue which is the compressive buckling load (P_o) or torsional buckling load (Q_s) depending on types of buckling of interest. Fourteen eigenvalues are obtained after the generalized eigenvalue problem shown in eq(4.10) is solved. The lowest eigenvalue is the buckling load for buckling

mode n. The corresponding eigenvector can be substituted into the approximate displacement function which is then plotted for buckling mode. The calculation is repeated for other buckling modes, i.e. other values of n. The lowest eigenvalue from each buckling mode is the theoretical buckling load of the annular plate and its corresponding value n is the buckling mode. Fig. 4.2 shows contour plots for buckling mode 4 and mode 7 of the compressive and torsional buckling.

4.3. Theoretical verification of rectangular plates

In this section, the scaling laws of symmetrical rectangular composite plates are verified using the solutions derived in the previous sections. The buckling load of a model is analytically or numerically determined and used as $(N_{xx})_m$ in the scaling law to predict the buckling load of the corresponding prototype, $(N_{xx})_p$. The scaling buckling load is then compared to the theoretical solution to determine the accuracy of the scaling law. Both complete similitude and partial similitude cases are included.

Complete similitude

The scaling law shown in eq(3.14) was examined by applying to the buckling problem of cross-ply laminated plates studied by Tuttle *et al.* [26]. Suppose the [0/90]_{2s} specimens used in that study were chosen as models in the present study. The buckling loads were theoretically determined from eq(4.1) and verified with the previous experimental study as shown in the 3rd and 4th column of Table 4.1, respectively. The next column compares theoretical and experimental results in term of percentage of discrepancy. In the current study, a prototype was selected as plates with the same stacking sequence and thickness as those of the model but have bigger dimensions. Specifically, the width of the model is 152.4 mm and the width of the prototype is 762

mm. Thus, the length and width of the prototype are five times larger than those of the model. Buckling loads for various plate configurations are illustrated in the last two columns of Table 4.1. Buckling loads determined from closed-form solution, eq(4.1), are shown in the "Theory" column and buckling loads obtained from similitude invariant or scaling law are shown in the last column entitled "Similitude." Since the stacking sequences of the models and the prototypes are identical, i.e. $C_{Dij} = C_{stiff} = 1$, the scaling law is simplified to

$$(N_{xx})_p = (N_{xx})_m \frac{b_m^2}{b_p^2} = \frac{1}{25} (N_{xx})_m$$

It should be emphasized that $(N_{xx})_m$ was a buckling load of the model based on the closed-form solution. For example, $(N_{xx})_p$ for a plate with aspect ratio of 1.5 without transverse tension was predicted from the scaling law as $(N_{xx})_p = \frac{1}{25} \times 24.2 = 0.968$ which is the same as that of calculated from theory. Also, the buckling loads of all other prototypes determined from the scaling law agree exactly with the results from theory. If buckling loads of prototypes $(N_{xx})_p$ were calculated from the test model data shown in the 4th column, the percent discrepancies would have been equal to those of the experiment in Ref [26].

Although D_{16} and D_{26} are not vanished for angle-ply laminates, complete similarity requirement can be achieved if the scaling factors of all laminate flexural stiffnesses are equal. Table 4.2. shows identical buckling loads determined from the scaling law and from theory for prototypes with 762-mm width. The models have identical stacking sequence, $[\pm 45]_{2s}$, with five times smaller than the prototypes.

As mentioned before that similarity conditions are independent of ply thickness, therefore similarity conditions are independent of ply thicknesses shall be investigated. Let select an eight-ply- $[0/90]_{2s}$ laminate as a model and consider two sixteen-ply laminates i.e. $[0_2/90_2]_{2s}$ and $[0/90]_{4s}$ as prototypes. The $[0_2/90_2]_{2s}$ prototype can be considered having the same stacking sequence as the model with twice ply thickness. All laminate flexural stiffnesses of $[0_2/90_2]_{2s}$ are eight times higher than their respective model stiffnesses, i.e. $C_{Dij} = 8$ as shown in Table 4.3. But the stiffnesses of the $[0/90]_{4s}$ prototype do not increase proportionally comparing with stiffnesses of the model. It was indicated in the previous section that constant C_{Dij} is required for complete similarity. In Table 4.4, buckling loads of the prototypes $[0_2/90_2]_{2s}$ and $[0/90]_{4s}$ laminates were determined from the scaling law using theoretical solution of $[0/90]_{2s}$ as models. They were then compared to the theoretical solutions. The "% Dis" column indicates discrepancies in percents between results from the scaling law and from theory. The similitude concept predicts buckling loads that exactly match the theoretical solution for $[0_2/90_2]_{2s}$. However, the $[0/90]_{4s}$ prototypes do have discrepancies because all C_{Dij} are not equal. Therefore the average value of C_{Dij} is used as C_{stiff} . It is seen that the variations of percent discrepancy are up to 13%.

In conclusion the complete similitude is obtained if two requirements, namely geometrical similarity and equality of all flexural stiffness scaling factors, are fulfilled. The buckling loads obtained from similitude theory for complete similarity cases show exact agreement to the solutions from analytical analysis. If any of similitude requirements is violated, the presented theory may be applied with some degree of discrepancies. The theory is then called approximate or partial similitude.

Partial similitude

Similitude invariant gives perfect solution for complete similitude cases, as previously mentioned. However, in some cases only partial similarity may be achieved

using distorted models as shown in Table 4.4 where $[0/90]_{4s}$ prototype are modeled from $[0/90]_{2s}$ laminates. Because the scaling factors for all stiffnesses are not identical, scaling law cannot be directly applied. If the equality of scaling factor is relaxed and the average of the stiffness scaling factors is used as C_{stiff} , the buckling load of $[0/90]_{4s}$ prototype could be determined. The discrepancies compared to the closed-form solution still show good agreement within $\pm 13\%$ as shown in Table 4.4.

Another examples of distorted model in number of plies are demonstrated in Table 4.5(a) and 4.5(b). The buckling loads of 304.8×152.4 mm² plates with $[\pm 45]_{ns}$ stacking sequences are determined from the Ritz method and compared to the similitude model. Stacking sequences of models were selected as $[\pm 45]_{4s}$ and $[\pm 45]_{7s}$ as shown in Table 4.5 (a) and 4.5(b) respectively. In both cases, scaling factors of all stiffnesses are not identical, however, they are divided into two groups. A group of C_{D11} , C_{D12} , C_{D22} and C_{D66} has the same value but different from the other group of C_{D16} , and C_{D26} . By using the value of the first group as C_{stiff} , the predicted buckling loads using the scaling laws show very good agreement with discrepancies less than 6%, except the first prototype with four plies. Hence, it can be concluded that as the number of plies exceeds eight, the effect of twisting coupling stiffness, D_{16} , and D_{26} , dies out rapidly and the approximate similitude calculation can consider only C_{D11} (= C_{D12} = C_{D22} = C_{D66}) as C_{stiff} .

Modeling a prototype from a model with different material is also possible by using the distorted model. This concept of distortion in material is very useful in minimizing cost of the test models. The possibility of this modeling is shown in Table 4.6-4,8. In Table 4.6., $[0/90]_{2s}$ graphite/epoxy prototype laminates were modeled from E-Glass/Epoxy laminates with the same stacking sequences and plate geometries using average value of C_{Dij} . The discrepancies of similitude model as compared to the theoretical solution are in the range of -13.5% to -27.2%. These discrepancies are fairly

high because the four values of C_{Dij} are quite different. Specifically C_{D11} and C_{D22} are approximately three times higher than C_{D12} and C_{D66} . In order to minimize the discrepancy, material of the model should be selected such that the differences in value of C_{Dij} are at minimum. Mechanical ply properties of both laminates used in this study are shown in Table 4.9.

Table 4.7 shows a more complicated study than that of in Table 4.6. Instead of having identical dimension of model and prototype as the previous study, the same models were employed to predicted prototypes with a larger size. Thus differences between the model and the prototype were not only types of material but also specimen dimensions. Discrepancies in this study are exactly the same as the case of different materials with the same plate dimension. A further study, which includes a change of stacking sequence, is shown in Table 4.8. Using the same $[0/90]_{2s}$ E-Glass/epoxy laminates with b = 152.4 mm, the buckling loads of $[0_2/90_2]_{2s}$ graphite/epoxy laminates with b = 762mm were predicted. The differences between model and prototype include material, dimension, and stacking sequence. However, only the distortion in material properties violate the scaling law, thus, the percent discrepancies remain the same as in Table 4.6 and 4.7.

4.4 Theoretical verification of annular plates

Similar to the rectangular plate, the scaling law for annular plate is also verified with the known solution. Both complete similitude and partial similitude are investigated using the same approach as that of the previous section.

Complete similitude

In this section, the scaling laws shown in eq(3.22) and eq(3.24) are verified using the theoretical solution discussed in the previous chapter. Solutions of both model and

prototype are determined from the Ritz method and considered as theoretical solutions. The theoretical solution of the model is then substituted into the scaling law to predict the similitude buckling load of the prototype. The accuracy of the scaling law is determined by comparing the similitude buckling load of the prototype to that of the theoretical solution. Table 4.10 shows mechanical properties of materials used in this study which include both composite materials and isotropic materials. The accuracy of the scaling law for compressive buckling is demonstrated in Table 4.11. A set of 6-mm thick annular plates with 400-mm outside diameter is selected as prototypes. Their buckling behaviors are predicted by the derived scaling law using theoretical solutions of the models. The thickness of the models is 3 mm which is a half of the prototype thickness, while other dimensions are the same. The first column of Table 4.11 shows the ratio of the inner radius to the outer radius. The ratio of inner pressure to outer pressure for each case of study is presented in the next column. Load ratio of 0, 0.5, 1, and 1.5 are used in this study. The 3rd and 4th columns are theoretical buckling load and mode of the models determined from the Ritz method. Similarly, the next two columns demonstrate the theoretical buckling behaviors of the prototypes. The last column labeled as "Similitude buckling load" is the buckling load of the prototypes $(P_o)_p$ calculated from the scaling law by substituting the theoretical buckling load of the model $(P_o)_m$ into the scaling law. Since both model and prototype are made from the same materials, all of the stiffness scaling factors are identical and equal to 8. Along with the complete geometric similarity and identical load ratio between the model and the prototype, both systems have complete similarity. Thus, the derived scaling law is applicable and is confirmed by the numerical comparison in Table 4.11. The similitude buckling loads in the last column agree exactly with the theoretical solutions. For buckling mode, similitude transformation implies that the buckling modes of the model and the prototype with complete similarity are identical.

Thus, similitude buckling modes of the prototype is not shown in the table because they are identical to those of shown in column 4. It is seen that the buckling mode is also well predicted using the similitude transformation.

Another study for model-prototype pairs with different size and thickness is presented in Table 4.12. Prototypes are selected as 5-mm-thick graphite-epoxy annular plates with 400-mm diameter. The buckling behaviors of the prototypes are modeled using smaller and thinner models with a diameter of 200 mm and a thickness of 3 mm. Complete similitude requirements are also satisfied, i.e. the scaling law is applicable. The numerical result shown in the table confirms the accuracy of the scaling law. Both buckling load and mode of the prototypes are accurately predicted.

The scaling for torsional buckling is verified in Table 4.13 with a similar approach. The complete similitude case is considered similar to the compressive buckling case. Material properties of graphite-epoxy are used in this case of study. Smaller and thinner annular plates are used to model the prototype plates. The theoretical torsional buckling loads of the model $(Q_s)_m$ are substituted in the torsional buckling scaling law, eq (3.24). The scaling law predicts the similitude buckling load which is very well matched the theoretical solutions. Like the compressive buckling case, the buckling mode is very well predicted using the derived scaling law.

In conclusion, the scaling laws for both compressive and torsional buckling of polar orthotropic annular plates are verified using the Ritz solution as a theoretical solution. Both buckling load and mode of the model-prototype pair are studied. For complete similitude cases, the derived scaling laws predict the buckling behaviors of the prototype very well.

Partial similitude

As shown, scaling law is very powerful and accurate for problems with complete similarity. However, it is not always practical or economical to set an experiment on the model such that the prototype is modeled with complete similarity. The scaling law would be more versatile if it could be applied to problems which some of the similarity requirements can be relaxed. This approach is called the "partial similitude" which is very practical, provided that the error caused by disregarding the similarity criterions can be assessed in advance. In this section, the partial similitude model is tested by selecting the model/prototype pairs such that the complete similitude is not fulfilled. The similarity requirements, which might be ignored, include the geometric similarity, identical load ratio, and identical stiffness scaling factor. It can be shown that the first two requirements are very essential for the similitude transformation. Numerical studies confirmed that partial similitude model ignoring either geometric similarity or load ratio requirement results in erroneous scaling law. Thus, disregarding those two similarity conditions is not recommended.

The partial similitude in stiffness scaling factor is the last similarity requirement which could possibly be neglected. The scaling law applied to a set of models and prototypes with non-uniform stiffness scaling factors is presented in Table 4.14. From the definitions of flexural stiffness, all the stiffness scaling factors are not identical if the ratio of radial modulus, tangential modulus, and shear modulus of the model to those of the prototype are different. In this study, E-glass/epoxy annular plates are employed as models to predict graphite/epoxy prototypes. Dimensions of the models and prototypes are selected to be the same so that the geometric similarity is satisfied. Only the uniqueness requirement among all the stiffness scaling factors is not achieved. The stiffness scaling factors are as followed: $C_{Dr} = 3.386$, $C_{D\theta} = 1.293$, $C_{Dr\theta} = 1.364$,

 $C_{D1} = 1.194$. By neglecting that requirement, the theoretical buckling load and mode are substituted into the scaling law to determine the similitude buckling load and mode of the prototype. The value of C_{stiff} in the scaling law is determined from the average value of the entire stiffness scaling factors which is 1.809. The similitude buckling load of the prototype is significantly different when compared with the theoretical solution. The percent discrepancy between the theoretical and similitude solutions ranges from -8 to -27 which is not only high but scattered. It would be difficult to indicate the accuracy of the scaling law in this case of partial similitude because of the scattering percent of discrepancy. Similarly, the buckling mode is not well predicted by the scaling law, as shown in the table. Therefore, the partial similitude model in material properties is not recommended similar to the partial similitude models in geometric similarity or load ratio. Further analysis shows that stiffness scaling factors are different from each other because of the anisotropic properties of material, i.e. difference of modulus in the r and θ direction.

It is interesting to apply the scaling law to an isotropic model/prototype pair since the modulus of elasticity is identical in all directions for isotropic material. The scaling law is applied to isotropic annular plates as shown in Table 4.15. The stainless steel prototype plates are modeled by aluminum plates. The material properties of both samples are shown in Table 4.10. The scaling law is proved to be accurate for this case of study. The similitude buckling loads are very well compared with the theoretical solution, i.e. percent discrepancy of less than 1%. The buckling modes determined from both approaches are identical. The partial similitude in this case results in an accurate scaling law because all the stiffness scaling factors are very close to each other. They are $C_{Dr} = C_{D\theta} = C_{D1} = 2.877$, and $C_{Dr\theta} = 2.857$ which are more uniform than those of the orthotropic material. It should be noted that a pair of isotropic model and prototype could

be modeled with complete similitude if their Poisson's ratios are the same and the shear modulus G is related to the Young's modulus E according to

$$G = \frac{E}{2(1+v)} \tag{4.11}$$

The exact agreement between similitude and theoretical solutions is not obtained in this case because the shear modulus employed in the study is not related to other mechanical properties according to eq(4.11). The scaling factor of $D_{r\theta}$ is different for those of the other stiffnesses.

In this chapter, the derived scaling laws for rectangular and annular plates are verified with available solutions. For all cases of complete similitude, the predicted buckling loads of the prototypes determined from the theoretical buckling loads of the models and the derived scaling law are identical to the theoretical solutions. It is observed that the experimental buckling loads of rectangular plates performed by Tuttle *et al.* [26] showed rather large discrepancies. One of the main causes of discrepancies is probably due to the fact that the experiment setup could not simulate the theoretical boundary conditions with sufficient accuracy. But the scaling laws will allow us to design experiments to simulate the condition of real application of the prototype without having to stick to the classical boundary conditions from theory. Hence, the application of the similitude theory appropriately can help cost and time savings in designing experiments of the complex unknown phenomena without the need for the solutions of the complicate differential equations while at the same time can predict the results according to the actual condition.

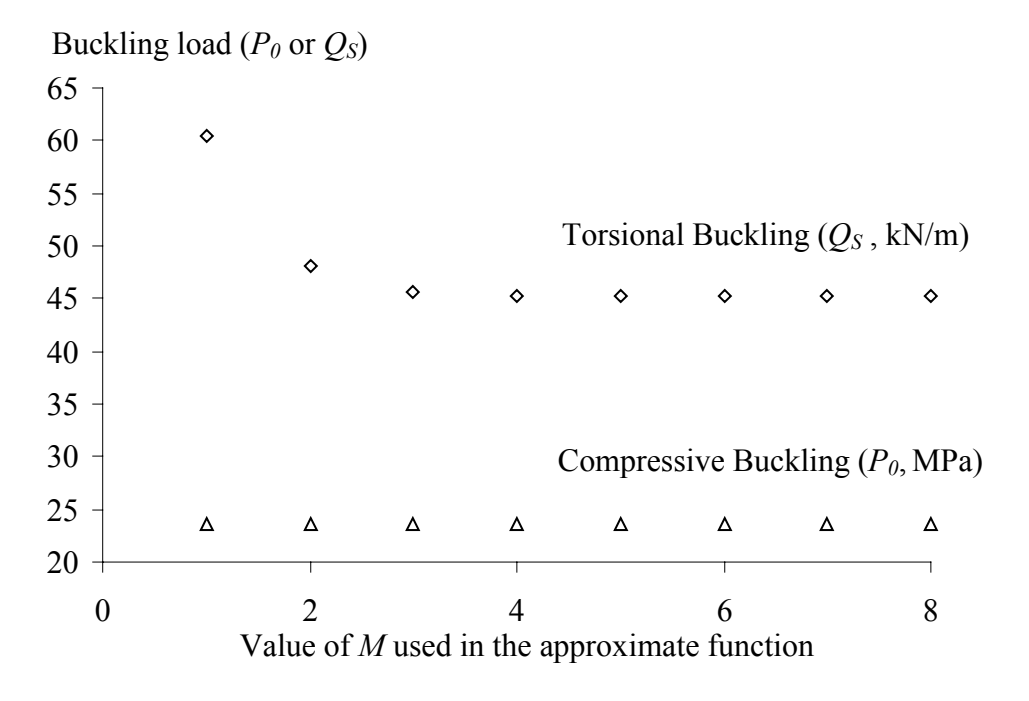


Fig 4.1. Convergence study for compressive and torsional buckling

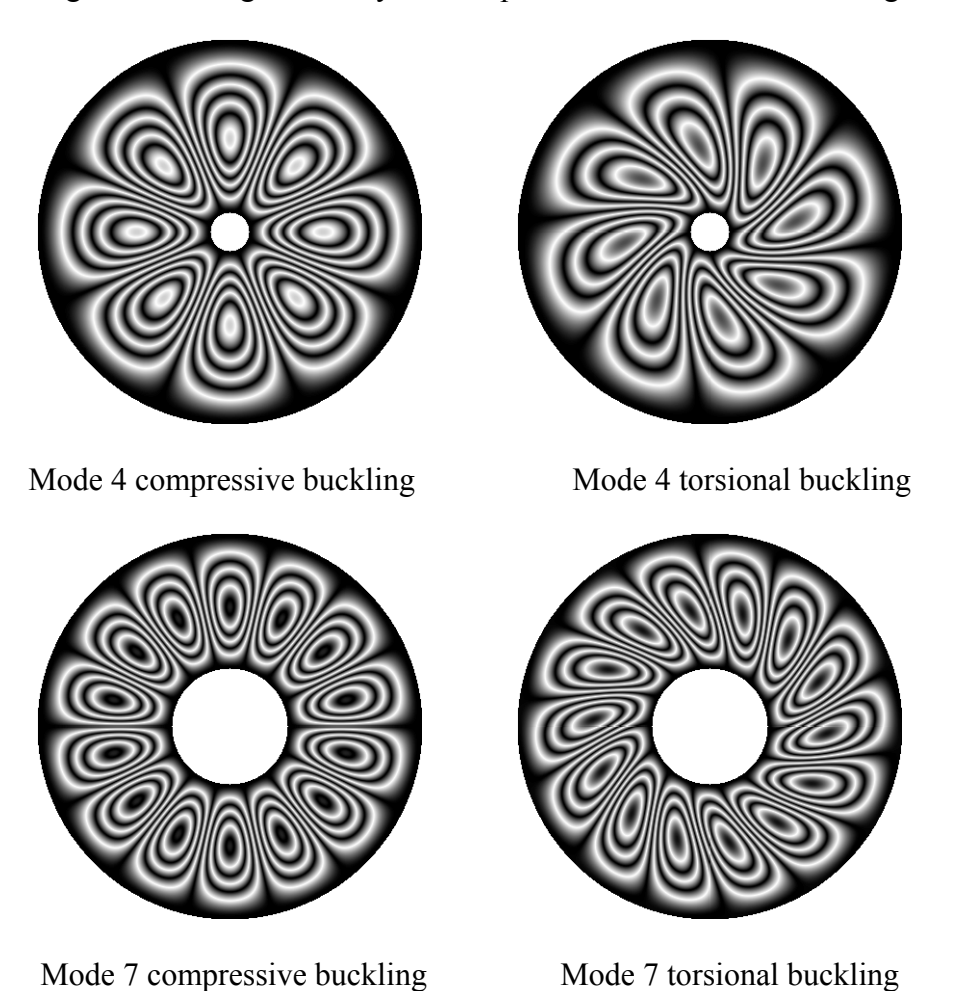


Fig 4.2. Out-of-plane displacement contour of buckling mode 4 and 7

Table 4.1 Buckling loads of $[0/90]_{2s}$ laminated plates determined from theory and scaling law.

Config	Configuration			Model		Prototype,	
		(b =	= 152.4 mm)		(<i>b</i> =	762 mm)	
Aspect	Load	Theory, N_{xxm}	Experiment	%Dis. in	Theory	Similitude,	
Ratio	Ratio	(kN/m)	(kN/m)	Exp	(kN/m)	N_{xxp} * (kN/m)	
	0	23.3	36.2	-35.6	0.935	0.935	
	-0.384	37.9	49.8	-23.9	1.52	1.52	
1	-0.587	56.5	58.0	-2.59	2.26	2.26	
	-0.688	71.8	N/A	N/A	2.87	2.87	
	0	24.2	28.2	-14.2	0.968	0.968	
	-0.384	39.6	42.4	-6.60	1.59	1.59	
1.5	-0.587	46.3	47.3	-2.11	1.86	1.86	
	-0.688	50.6	48.9	3.48	2.03	2.03	
	0	23.3	21.2	9.91	0.935	0.935	
	-0.384	37.9	42.9	-11.7	1.52	1.52	
2	-0.587	49.7	54.1	-8.13	2.00	2.00	
	-0.688	52.9	55.3	-4.34	2.12	2.12	

*
$$N_{xxp} = N_{xxm} \left(\frac{b_m}{b_p}\right)^2$$

Table 4.2 Buckling loads of $[\pm 45]_{2s}$ laminated plates determined from theory and similitude

Config	uration	Model	Prototype (b	p = 762 mm
Aspect	Load	(b = 152.4 mm)	Theory	Similitude
Ratio	Ratio	(kN/m)	(kN/m)	(kN/m)
	0	39.32	1.57	1.57
	-0.3	55.78	2.23	2.23
1	-0.6	60.99	2.44	2.44
	0	40.71	1.63	1.63
	-0.3	49.31	1.97	1.97
1.5	-0.6	60.97	2.44	2.44
	0	38.87	1.55	1.55
	-0.3	49.53	1.98	1.98
2	-0.6	58.92	2.36	2.36

1 able 4.3 C_{Dii} of $ 02/902 _{2s}$ and $ 0/90 _{4s}$ plates having $ 0/90 _{2s}$ as a mod	able 4.3 C_{Dij} of $[0_2/90_2]_{2s}$ and $[0/90]_{4s}$ pla	tes having $[0/90]_{2s}$ as a mode
---	--	------------------------------------

	Model	Prototype				
		$[0_2/90$	$[2]_{2s}$	$[0/90]_{4s}$		
	$[0/90]_{2s}$	D_{ij} (Gpa-mm ³)	C_{Dij}	D_{ij} (Gpa-mm ³)	C_{Dij}	
D_{11}	32.34	258.7	8	225.9	6.985	
D_{12}	0.7649	6.119	8	6.119	8	
D_{22}	15.93	127.4	8	160.2	10.06	
D ₆₆	1.302	10.41	8	10.41	8	

Table 4.4 Scaling law applied to laminated plates having different ply thickness and stacking sequences.

Agmost	Lood	Buckling load [0/90] _{2s}	Buckling load of prototype (kN/m)						
Aspect ratio	Load ratio	Model		$[0_2/90_2]_{2s}$			$[0/90]_{4s}$] _{4s}	
Tatio	Tallo	(kN/m)	Theory	Similitude	% Dis.	Theory	Similitude*	% Dis.	
	0	4.09	32.75	32.75	0.00	32.75	33.79	3.17	
1	-0.384	6.65	53.16	53.16	0.00	53.16	54.94	3.34	
1	-0.587	9.91	79.29	79.29	0.00	79.29	81.87	3.25	
	0	4.24	33.90	33.90	0.00	38.31	35.03	-8.57	
1.5	-0.384	6.95	55.58	55.58	0.00	51.79	57.42	10.9	
1.3	-0.587	8.13	65.05	65.05	0.00	60.62	67.16	10.8	
	0	4.09	32.75	32.75	0.00	32.75	33.79	3.17	
2	-0.384	6.65	53.16	53.16	0.00	53.16	54.94	3.34	
2	-0.587	8.72	69.74	69.74	0.00	63.77	72.04	13.0	

^{*} Calculated base on $C_{stiff} = \frac{C_{D11} + C_{D12} + C_{D22} + C_{D66}}{4} = 8.261$

Table 4.5(a) Buckling loads of $[\pm 45]_{ns}$ having $[\pm 45]_{4s}$ as a model

Value of n	Scaling Factor	Buckling load (kN/m)		
in [±45] _{ns}	$C_{D11}, C_{D12}, C_{D22}, C_{D66} : C_{D16}, C_{D26}$	Ritz Method	Similitude	% Dis.
	21. 21. 22. 22. 200 210 220		$(C_{stiff} = C_{D11})$	
1	0.015625 : 0.0625	3.887	5.062	30.2
2	0.125 : 0.25	38.87	40.50	4.20
3	0.421875 : 0.5625	135.3	136.7	1.03
4(model)	-	324.0	1	-
5	1.953125 : 1.5625	635.7	632.8	-0.47
6	3.375 : 2.25	1101	1093	-0.72
7	5.359375 : 3.0625	1751	1736	-0.87

Table 4.5(b) Buckling loads of $[\pm 45]_{ns}$ having $[\pm 45]_{7s}$ as a model

Value of n	Scaling Factor	Buckling load (kN/m)		
in [±45] _{ns}	$C_{D11}, C_{D12}, C_{D22}, C_{D66} : C_{D16}, C_{D26}$	Ritz Method	Similitude	% Dis.
			$(C_{stiff} = C_{D11})$	
1	0.0029 : 0.0204	3.887	5.107	31.4
2	0.0233 : 0.0816	38.87	40.85	5.11
3	0.07872 : 0.1837	135.3	137.9	1.92
4	0.1866 : 0.3265	324.0	326.8	0.875
5	0.3644 : 0.5102	635.7	638.3	0.404
6	0.6297 : 0.7347	1101	1103	0.151
7(model)	-	1752	-	-

Note : a = 304.8 mm, b = 152.4 mm. Load ratio = 0

Table 4.6 Buckling loads of $[0/90]_{2s}$ graphite/epoxy laminates(b = 152.4 mm) modeled from E-glass/epoxy laminates (b = 152.4 mm)

Configuration		Model (E-Glass/Epoxy)	Prototype (Graphite/Epoxy		poxy)
Aspect	Load	Theory, N _{xxm}	Theory	Similitude*	0/ Dia *
Ratio	Ratio	(kN/m)	(kN/m)	(kN/m)	% Dis.*
	0	8.584	23.37	19.23	-17.7
	-0.3	12.26	33.39	27.47	-17.7
1	-0.6	21.18	58.43	47.46	-18.8
	0	9.349	24.20	20.94	-13.5
	-0.3	12.61	37.42	28.24	-24.5
1.5	-0.6	15.82	46.95	35.43	-24.5
	0	8.584	23.37	19.23	-17.7
	-0.3	12.26	33.39	27.47	-17.7
2	-0.6	16.31	50.17	36.54	-27.2

* Calculated base on
$$C_{stiff} = \left(\frac{C_{D11} + C_{D12} + C_{D22} + C_{D66}}{4}\right) = \left(\frac{3.71 + 1.19 + 3.00 + 1.07}{4}\right) = 2.24$$

Table 4.7 Buckling loads of $[0/90]_{2s}$ graphite/epoxy (b=762mm) laminates modeled from E-glass/epoxy laminates (b=152.4 mm)

Configu	uration	Model (E-Glass/Epoxy)	Prototype (Graphite/Epoxy)		
Aspect	Load	Theory, N _{xxm}	Theory	Similitude*	% Dis.*
Ratio	Ratio	(kN/m)	(kN/m)	(kN/m)	70 DIS.
	0	8.584	0.9350	0.7693	-17.7
	-0.3	12.26	1.336	1.099	-17.7
1	-0.6	21.18	2.337	1.898	-18.8
	0	9.349	0.9680	0.8378	-13.5
	-0.3	12.61	1.497	1.130	-24.5
1.5	-0.6	15.82	1.878	1.417	-24.5
	0	8.584	0.9350	0.7693	-17.7
	-0.3	12.26	1.336	1.099	-17.7
2	-0.6	16.31	2.007	1.462	-27.2

* Calculated base on
$$C_{stiff} = \left(\frac{C_{D11} + C_{D12} + C_{D22} + C_{D66}}{4}\right) = \left(\frac{3.71 + 1.19 + 3.00 + 1.07}{4}\right) = 2.24$$

Table 4.8 Buckling load of $[0_2/90_2]_{2s}$ graphite/epoxy prototype (b=762mm) and $[0/90]_{2s}$ E-glass/epoxy model (b=152.4 mm)

Configu	uration	Model (E-Glass/Epoxy)	Prototype (Graphite/Epox		oxy)
Aspect	Load	Theory, N _{xxm}	Theory	Similitude*	% Dis.*
Ratio	Ratio	(kN/m)	(kN/m)	(kN/m)	/0 DIS.
	0	8.584	7.480	6.154	-17.7
	-0.3	12.26	10.69	8.792	-17.7
1	-0.6	21.18	18.70	15.19	-18.8
	0	9.349	7.744	6.702	-13.5
	-0.3	12.61	11.97	9.037	-24.5
1.5	-0.6	15.82	15.02	11.34	-24.5
	0	8.584	7.480	6.154	-17.7
	-0.3	12.26	10.69	8.792	-17.7
2	-0.6	16.31	16.05	11.69	-27.2

^{*} Calculated base on

$$C_{stiff} = \left(\frac{C_{D11} + C_{D12} + C_{D22} + C_{D66}}{4}\right) = \left(\frac{29.67 + 9.505 + 23.98 + 8.533}{4}\right) = 17.9$$

Table 4.9 Ply properties of composites used in buckling of rectangular plate problems

	E ₁₁	E_{22}	G_{12}	v_{12}
	GPa (Msi)	Gpa (Msi)	GPa (Msi)	
Graphite/Epoxy	155 (22.5)	7.6 (1.1)	4.4 (0.64)	0.34
E-Glass/Epoxy	38.6 (5.6)	8.27 (1.2)	4.14 (0.6)	0.26

Table 4.10 Ply properties of composites used in analysis of annular plates

	E_{II}	E_{22}	G_{12}	v_{12}
	(GPa)	(GPa)	(GPa)	
Graphite/Epoxy	132	10.8	5.65	0.24
E-Glass/Epoxy	38.6	8.27	4.14	0.26
2014-T6 Al	73	73	28	0.3
Stainless steal	210	210	80	0.3

Table 4.11 Compressive buckling of 6-mm thick Graphite/epoxy annular plates determined from theory and from similitude (b = 200 mm)

Configuration		Model ($h = 3 \text{ mm}$)		Prototype, $(h = 6 \text{ mm})$			
Ratio	Load	Theoretical	Theoretical	Theoretical	Theoretical	Similitude	
of a/b	Ratio,	buckling load,	buckling	buckling load,	buckling	buckling	
	q	$(P_o)_m$, (MPa)	mode (n)	(MPa)	mode(n)	load, $(P_o)_p$	
						(MPa)	
	0	38.36	4	153.5	4	153.5	
0.1	0.5	39.62	4	158.5	4	158.5	
	1	40.96	4	163.8	4	163.8	
	1.5	42.39	4	169.6	4	169.6	
	0	50.90	7	203.6	7	203.6	
0.3	0.5	57.81	7	231.3	7	231.3	
	1	66.90	7	267.6	7	267.6	
	1.5	78.85	6	315.4	6	315.4	
	0	73.16	12	292.6	12	292.6	
0.5	0.5	93.85	12	375.4	12	375.4	
	1	130.8	12	523.2	12	523.2	
	1.5	208.3	10	833.4	10	833.4	

Table 4.12 Compressive buckling of Graphite/epoxy annular plates determined from model plates with different size and thickness

Configuration		Mode	el	Prototype			
		(b = 100 mm, b)	h = 3 mm	(b = 200 mm, h = 5 mm)			
Ratio	Load	Theoretical	Theoretical	Theoretical	Theoretical	Similitude	
of a/b	ratio,	buckling load,	buckling	buckling load,	buckling	buckling	
	q	$(P_o)_m$, (MPa)	mode (n)	(MPa)	mode(n)	load, $(P_o)_p$	
						(MPa)	
	0	153.5	4	106.6	4	106.6	
0.1	0.5	158.5	4	110.1	4	110.1	
	1 163.8		4	113.8	4	113.8	
	1.5	169.6	4	117.7	4	117.7	
	0	203.6	7	141.4	7	141.4	
0.3	0.5	231.3	7	160.6	7	160.6	
	1	267.6	7	185.8	7	185.8	
	1.5	315.4	6	219.0	6	219.0	
	0	292.6	12	203.2	12	203.2	
0.5	0.5	375.4	12	260.7	12	260.7	
	1 523.2 12		12	363.4	12	363.4	
	1.5	833.4	10	578.7	10	578.7	

Table 4.13 Torsional buckling of Graphite/epoxy annular plates determined from model plates with different size and thickness

Ratio	Mod	el	Prototype			
of a/b	(b = 200 mm,	h = 3 mm	(b = 1000 mm, h = 15 mm)			
	Theoretical	Theoretical	Theoretical	Theoretical	Similitude	
	buckling load,	buckling	buckling	buckling	buckling load,	
	$(Q_s)_m$, (kN/m)	mode(n)	load, (kN/m)	mode(n)	$(Q_s)_p$ (kN/m)	
0.1	56.32	4	281.6	4	281.6	
0.2	111.6	5	558.2	5	558.2	
0.3	198.5	7	992.7	7	992.7	
0.4	340.9	9	1704	9	1704	
0.5	594.6	11	2973	11	2973	

Table 4.14 Compressive buckling of Graphite/epoxy annular plates determined from E-Glass/Epoxy model.

Configuration		Model		Prototype				
		(E-Glass/Epoxy)		(Graphite/epoxy)				
Ratio	Load	Theoretical	Theoretical	Theoretical	Theoretical	Similitude	%Disc.	
of a/b	Ratio, q	buckling load,	buckling	buckling	buckling	buckling load,		
		$(P_o)_m$, (MPa)	mode(n)	load, (MPa)	mode(n)	$(P_o)_p$ (MPa)		
	0	17.20	3	38.36	4	31.13	-18.9	
0.1	0.5	17.58	3	39.62	4	31.82	-19.7	
	1	17.98	3	40.96	4	32.54	-20.6	
	1.5	18.40	3	42.39	4	33.29	-21.5	
	0	24.90	5	50.90	7	45.05	-11.5	
0.3	0.5	27.54	5	57.81	7	49.83	-13.8	
	1	30.80	5	66.90	7	55.73	-16.7	
	1.5	34.65	4	78.85	6	62.70	-20.5	
	0	36.94	10	73.16	12	66.83	-8.64	
0.5	0.5	46.20	9	93.85	12	83.60	-10.9	
	1	61.31	8	130.8	12	110.9	-15.2	
	1.5	84.27	6	208.3	10	152.5	-26.8	

Note: b = 200 mm, h = 3 mm

Table 4.15 Buckling of stainless steel annular plates determined from 2014-T6 Al model.

Configuration		Model (2014-T6 Al)		Prototype (Stainless steel)			
Ratio	Load	Theoretical	Theoretical	Theoretical	Theoretical	Similitude	%Disc.
of a/b	Ratio,	buckling load,	buckling	buckling	buckling	buckling load,	
	q	$(P_o)_m$, (MPa)	mode (n)	load (MPa)	mode (n)	$(P_o)_p$ (MPa)	
	0	66.93	2	192.3	2	192.2	-0.021
0.1	0.5	67.36	2	193.5	2	193.5	-0.021
	1	67.71	1	194.7	1	194.4	-0.104
	1.5	66.99	1	192.6	1	192.4	-0.104
	0	105.6	3	303.3	3	303.2	-0.025
0.3	0.5	110.0	3	316.1	3	316.0	-0.025
	1	112.2	2	322.4	2	322.1	-0.078
	1.5	110.8	1	318.6	1	318.1	-0.142
	0	171.1	6	491.3	6	491.2	-0.009
0.5	0.5	198.3	5	569.6	5	569.5	-0.023
	1	222.1	4	638.2	4	637.9	-0.052
	1.5	208.4	1	599.4	1	598.4	-0.159

Note: b = 200 mm, h = 3 mm